Adaptive regridding in 3D reflection tomography

Gualtiero Böhm, Giuliana Rossi and Aldo Vesnaver
Osservatorio Geofisico Sperimentale, Trieste, Italy

Abstract
3D reflection tomography allows the macro-model of complex geological structures to be reconstructed. In the usual approach, the spatial distribution of the velocity field is discretized by regular grids. This choice simplifies the development of the related software, but introduces two serious drawbacks: various domains of the model may be poorly covered, and a relevant mismatch between the grid and a complex velocity field may occur. So the tomographic inversion becomes unstable, unreliable and necessarily blurred. In this paper we introduce an algorithm to adapt the grid to the available ray paths and to the velocity field in sequence: so we get irregular grids with a locally variable resolution. We can guide the grid fitting procedure interactively, if we are going to introduce some geological *a priori* information; otherwise, we define a fully automatic approach, which exploits the Delauny triangles and Voronoi polygons.

Key words *reflection tomography – irregular grids – automatic regridding – travel time inversion*

1. Introduction

The estimate of the local velocity of seismic waves is a parametric inversion of their travel times. We assume first some general model for the Earth structure, characterised by a few free parameters; then we fit it to our experimental data by optimising these parameters, according to some physical or mathematical principles.

Often, the chosen Earth model is very simple, like a set of plane parallel layers of variable thickness. This is the case for the velocity spectra in reflection seismics (Taner and Köhler, 1969; Hubral and Krey, 1980), which provide a 1D function relating velocity and travel times. We can estimate more complicated 2D velocity models by allowing for the effects of possible dipping interfaces, *i.e.* by the Dip Move Out (DMO) correction (Yilmaz and Claerbout, 1980; Rocca *et al.*, 1982; Hale, 1983).

The tomographic inversion of travel times allows much more complex models for the Earth to be adopted, especially in 3D. In the most common approach, the investigated area is discretized by voxels, *i.e.* parallelepipeda where the physical properties are supposed constant in space (in 2D, they are often called pixels). Usually the voxel shape and size is the same everywhere, and so the velocity field is estimated in a regular grid. This choice is due to the much simpler software setting up of the tomographic inversion, but may lead to serious drawbacks. In fact, the distribution of the available ray paths may be quite uneven, and some voxels may be not crossed at all. These facts cause heavy instabilities and the non-uniqueness of solutions (Vesnaver, 1994).

Mailing address: Dr. Gualtiero Böhm, Osservatorio Geofisico Sperimentale, P.O. Box 2011, 34016 Trieste, Italy; e-mail: WALTER@REDS.OGS.TRIESTE.IT

An important advantage of seismic tomography over other inversion methods is the possibility of exploiting different wave types jointly and an arbitrary distribution of sources and receivers (see *e.g.*, Vesnaver, 1996).

In this paper we show that transmitted and reflected arrivals allow a complex 3D geological structure to be reconstructed. By adopting irregular grids in sequence, we match the local resolution to one that can be supported by the ray paths' distribution: so we obtain a reliable solution, which is not affected by the instabilities due to the null space of the tomographic equations. We also match the shape of the voxels in the chosen space discretization to the estimated velocity anomalies, and so we further reduce the estimate errors.

2. The principle of minimum dispersion

In the tomographic inversion of seismic velocities, the vector $\boldsymbol{t}$ of the measured travel times is related to the vector $\boldsymbol{u}$ of the unknown slownesses by a linear function:

$$\boldsymbol{t} = \boldsymbol{A}\,\boldsymbol{u}, \qquad (2.1)$$

where the tomographic matrix $\boldsymbol{A}$ depends on the ray paths of the considered waves.

The solution of (2.1) is rarely unique. Generally the system is rank deficient and a null space exists: we therefore obtain a space of solutions, instead of just one. Among the infinite possible ones, however, we can choose some of them satisfying further requirements. A very effective choice is that the vector $\boldsymbol{u}$ of unknown slownesses has a minimum energy (Menke, 1984; Carrion, 1991): in this way, the solution is unique and not contaminated by the null space.

From the practical point of view, we inverted system (2.1) by the SIRT method, based on the Kaczmarz' algorithm (Kaczmarz, 1937; van der Sluis and van der Vorst, 1987). Althought it is a bit slower than the ART approach, we preferred the SIRT one because it produces tomographic images that do not depend on the equation order in (2.1), *i.e.* that of the traced ray paths, as happens with ART. Furthermore, SIRT is more stable and robust: it may be generalized and applied even when the picked travel times are affected by experimental errors and some mispicks (Dobroka, 1994; Dobroka *et al.*, 1991).

System (2.1) yields a parametric inversion of slownesses $\boldsymbol{u}$ from travel times $\boldsymbol{t}$. We assume explicitly that the space properties are fairly well represented by voxels, *i.e.* that we can approximate the velocity field by a blocky function. Also, we assume implicitly that the reflecting (or refracting) interfaces are fixed and known, if we use reflected (or refracted) waves.

Naturally, often we do not know precisely (or at all) the shape and depth of the interfaces of the Earth layers. These additional unknowns aggravate the already ill-posed problem (2.1). Again, we can face the new degrees of freedom by adopting a further principle. Here we can exploit the natural lateral continuity of geological interfaces, as proposed by Carrion *et al.* (1993a,b), which is what we call the *principle of minimum dispersion.*

From the practical point of view, we can split the inversion procedure we propose into distinct parts. The estimate of the vertical and the lateral velocity gradient should be done separately, at the beginning, and jointly only at the end.

In the seismic exploration, the usual acquisition geometry allows for the multiple coverage of the reflecting points in depth (fig. 1). So we adopt first a local 1D model composed of horizontal layers. Our two unknowns are z and v, which are the reflector depth and the RMS velocity from surface to reflector, respectively; the data available in two dimensions are t and o, *i.e.* the travel times and the offsets between source and receiver. We can solve the unknowns t-v by scanning several possible couples at each reflector: the values t-v providing the minimum dispersion for the corresponding reflection points are the sought solution. So we satisfy a basic physical principle: the seismic waves are reflected at the surface because a notable change of the local physical properties occurs in a limited zone.

Repeating the estimate just described for each major reflector and at different places, we obtain a first image of the velocity field and re-

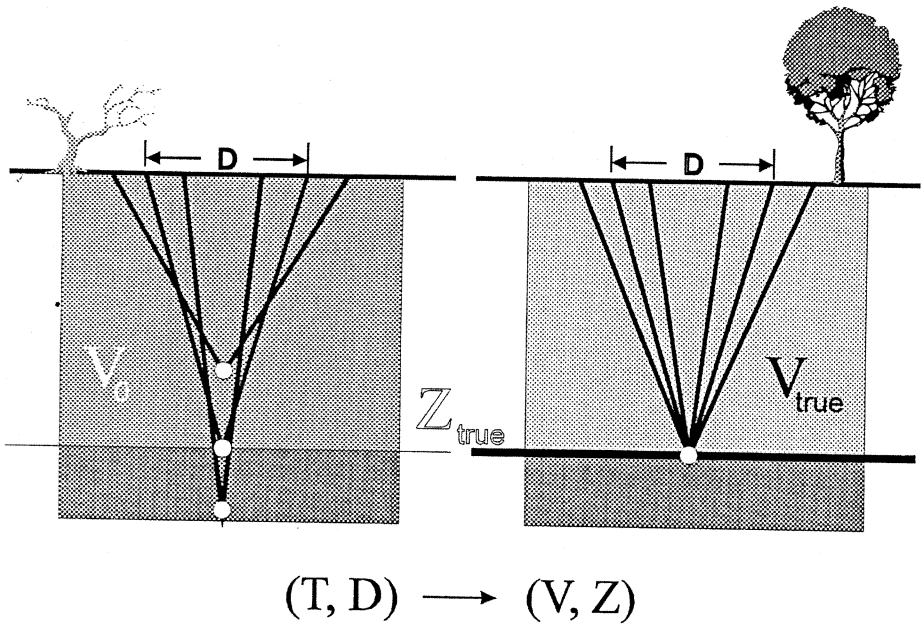

Fig. 1. The principle of minimum dispersion in a 1D model. We estimate the layers' velocity and thickness from the travel time variations with respect to the offset.

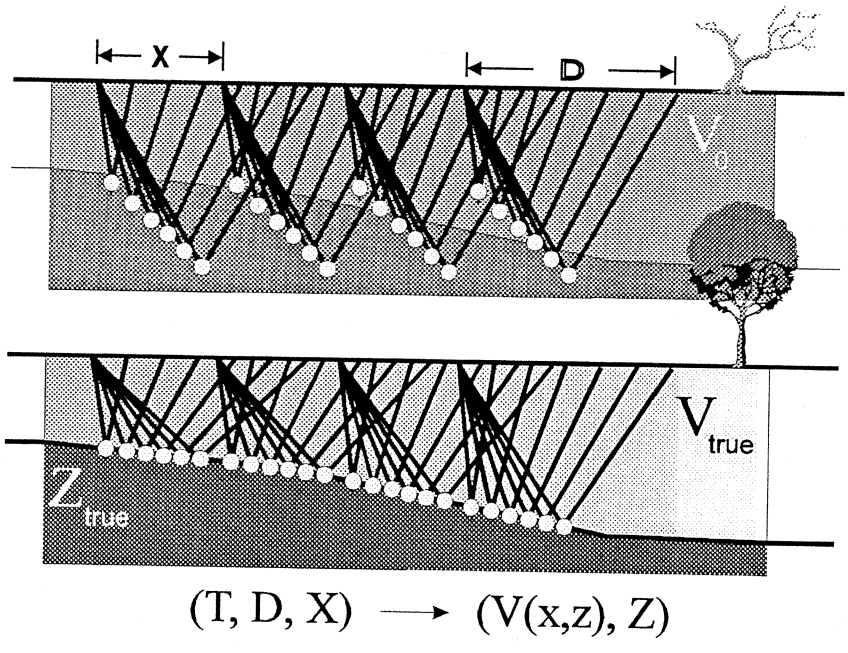

Fig. 2. The principle of minimum dispersion in a 2D model. We compute the lateral velocity variations in each layer by imposing the lateral continuity of the estimated reflectors.

flector structure in 2D or 3D. Naturally this guess may suffer from relevant errors, mainly when dipping interfaces are present. So a second application of the minimum dispersion principle is necessary: now, along the dimensions x and y, which are the spatial coordinates of the sources and receivers at the surface. Figure 2 shows a 2D example: we obtain the correct values of $v(x)$ when the dispersion of the estimated reflection points is small both vertically and laterally.

3. 3D reflection tomography

Figure 3 is a block diagram of the procedure we follow in practice for the 3D tomographic inversion. First, we select a few 2D profiles from the whole 3D data set, and obtain a preliminary 2D inversion as described in fig. 2. Secondly, we interpolate these profiles to 3D and obtain a first guess for the 3D velocity field and the reflecting surfaces. Then we invert the whole data set for the velocity field in 3D, leaving fixed the layer interfaces: so we consider the 3D geometry of the ray paths. Later, if necessary, we update further both the reflectors' shape and the velocity field in sequence, until their variations become small enough.

Figure 4 shows the model of a steep anticline, surrounded by a layered medium with dipping interfaces. At its top, we set a low velocity anomaly resembling a hydrocarbon reservoir. The model interfaces are characterised by a circular symmetry and are described by 2D spline functions.

In fig. 5 we see a few ray paths by a transparency effect, displaying some voxels. The small cubes at the model boundaries show the position of sources and receivers. We placed many sources and receivers at the surface, which are necessary to reconstruct the layer interfaces by the reflected waves. Furthermore, we introduced a few wells at the model boundaries and traced the ray paths of transmitted waves across them, to improve the voxel coverage in the outer domains.

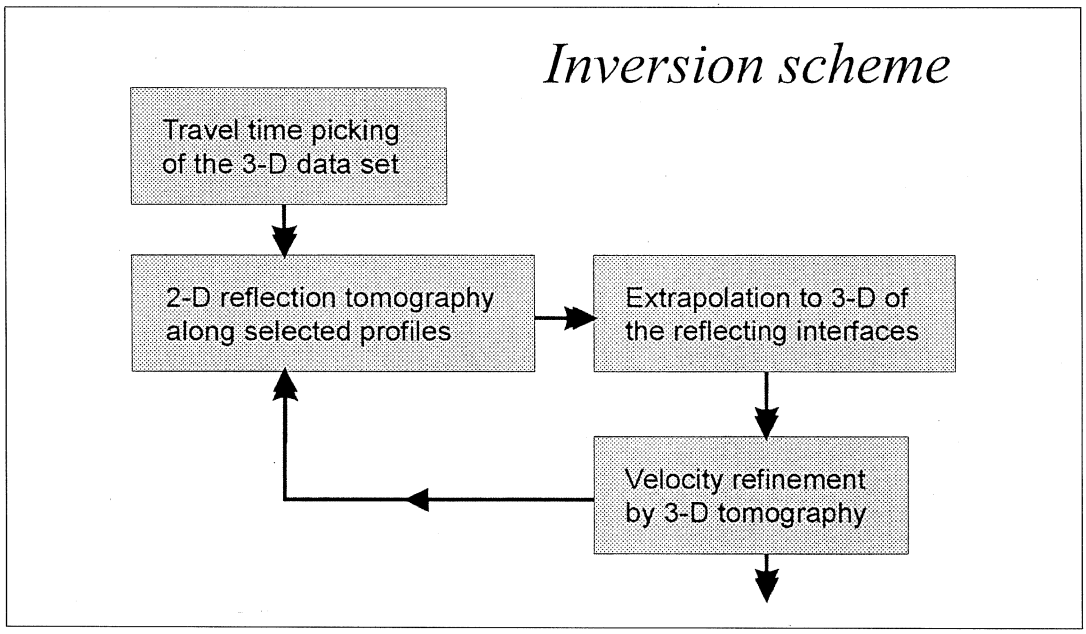

Fig. 3. Block diagram of the procedure for the 3D reflection tomography.

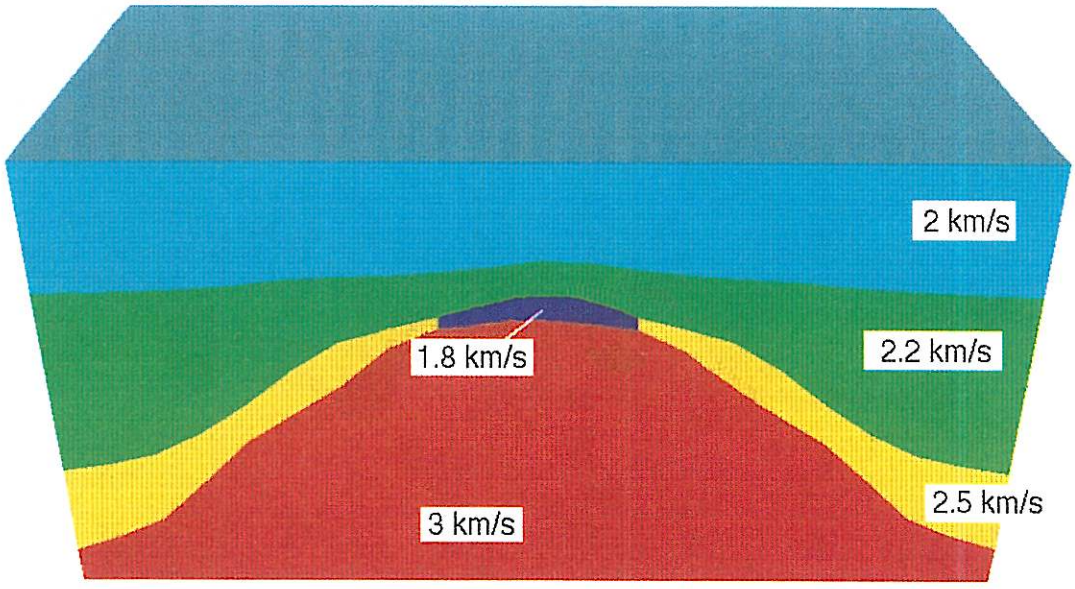

Fig. 4. 3D synthetic model of a steep anticline, with a low velocity anomaly at its top.

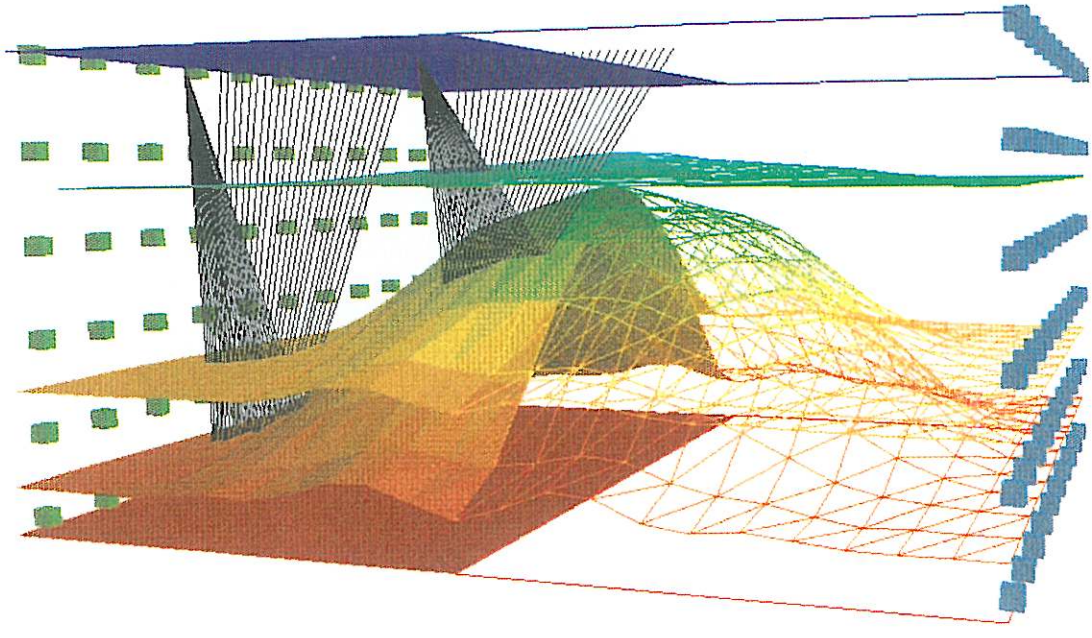

Fig. 5. A few ray paths across the model in fig. 4.

Figure 6 displays (at left) the first step of the inversion along a 2D profile to reconstruct the third interface. Starting with a wrong surface (green line) and a wrong velocity in the third layer (3.2 km/s), we obtain a large dispersion for the estimated reflection points. Their different colours denote their different offsets: from blue for the smallest ones to red for the largest. After some iterations, we obtain the desired minimum dispersion for all interfaces

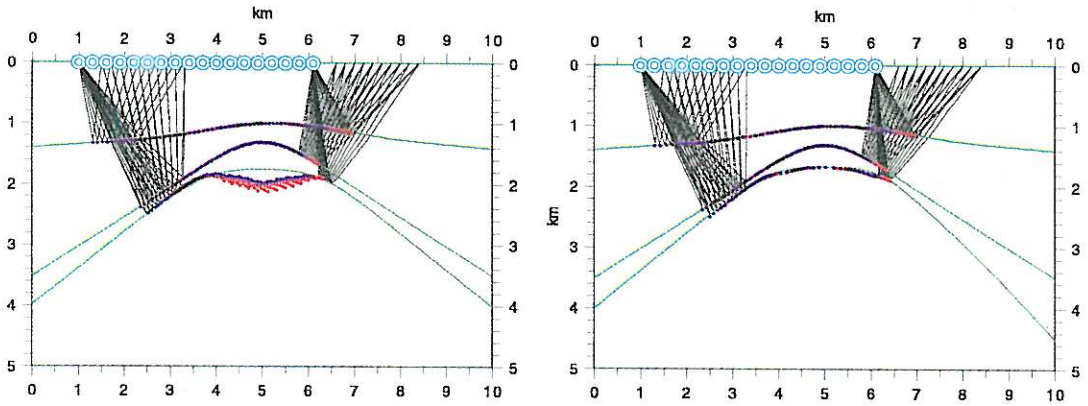

Fig. 6. First step (left) and final estimate (right) of the 2D reflection tomography procedure at the uppermost interface.

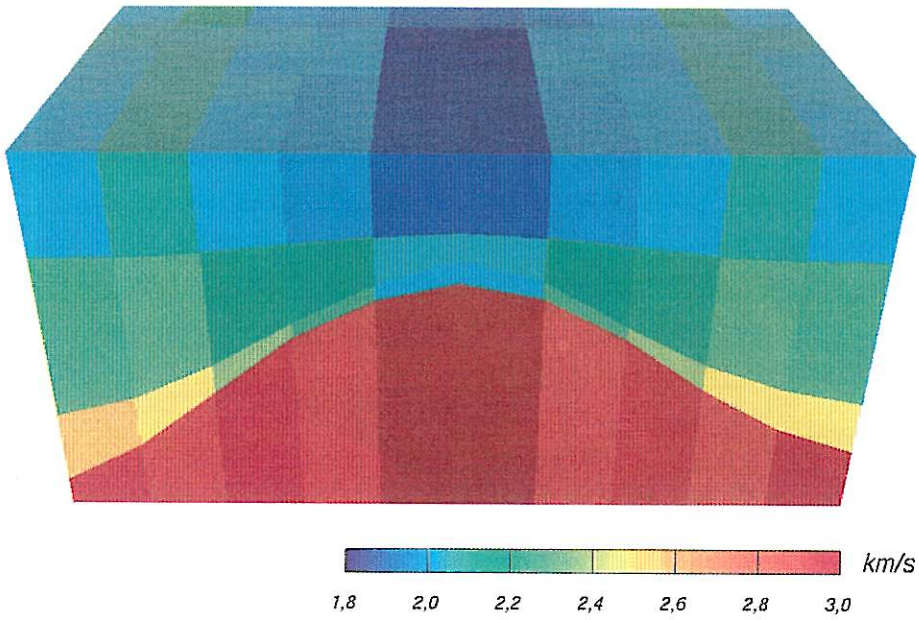

Fig. 7. Velocity field estimated by the 3D tomographic inversion using a nearly regular grid.

(fig. 6, at right): all points at different offsets provide the same image of the Earth.

We notice in fig. 6 that only the central part of the model is adequately covered, and that this coverage is poorer as the depth increases. This is due to the steep flanks of the anticline, which shift the reflection points towards the anticline top. As a result, the interfaces at the model boundaries are just extrapolated from the central part, and so their reliability is much lower.

Figure 7 shows the velocity field estimated by the tomographic inversion of reflected and transmitted arrivals using a nearly regular grid. The reconstruction is quite good in the central zone, and poorer elsewhere. This is mainly due to the not very precise reflectors' shape at the boundaries.

4. Regular and irregular grids

Our model is composed of a few homogeneous domains irregularly shaped. Let us suppose that this *a priori* information is available to us. (Naturally, this is not true in general; *vice versa*, sometimes the available independent information may be wrong, and so misleading). We can exploit this extra knowledge by adapting the grid to the velocity field estimated in sequence (Böhm and Vesnaver, 1996). Figure 8 shows the final result so obtained, that is very good and much closer to the actual model (fig. 4) than that provided by the conventional approach (fig. 7).

We can appreciate better the differences of these images by taking a horizontal slice at the level of the hydrocarbon trap (fig. 9, top). Looking at the image provided by the conventional approach (top, at right), we see that the zone surrounding the central anomaly is quite homogeneous, but the anomaly boundary is quite blurred. According to our *a priori* information we expect sharper boundaries, but we do not know their shape. So we merged the outer voxels into larger ones, and introduced smaller ones around the anomaly. Doing so (bottom, at left), its actual shape becomes much clearer. Our final step (bottom, at right), obtained by merging the unnecessary small

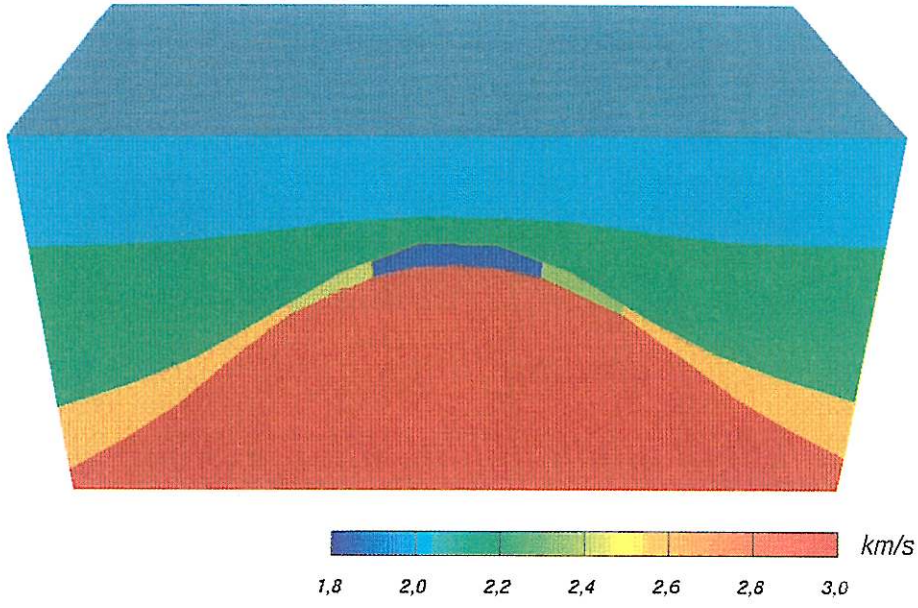

Fig. 8. Velocity field estimated by the 3D tomographic inversion using an irregular grid.

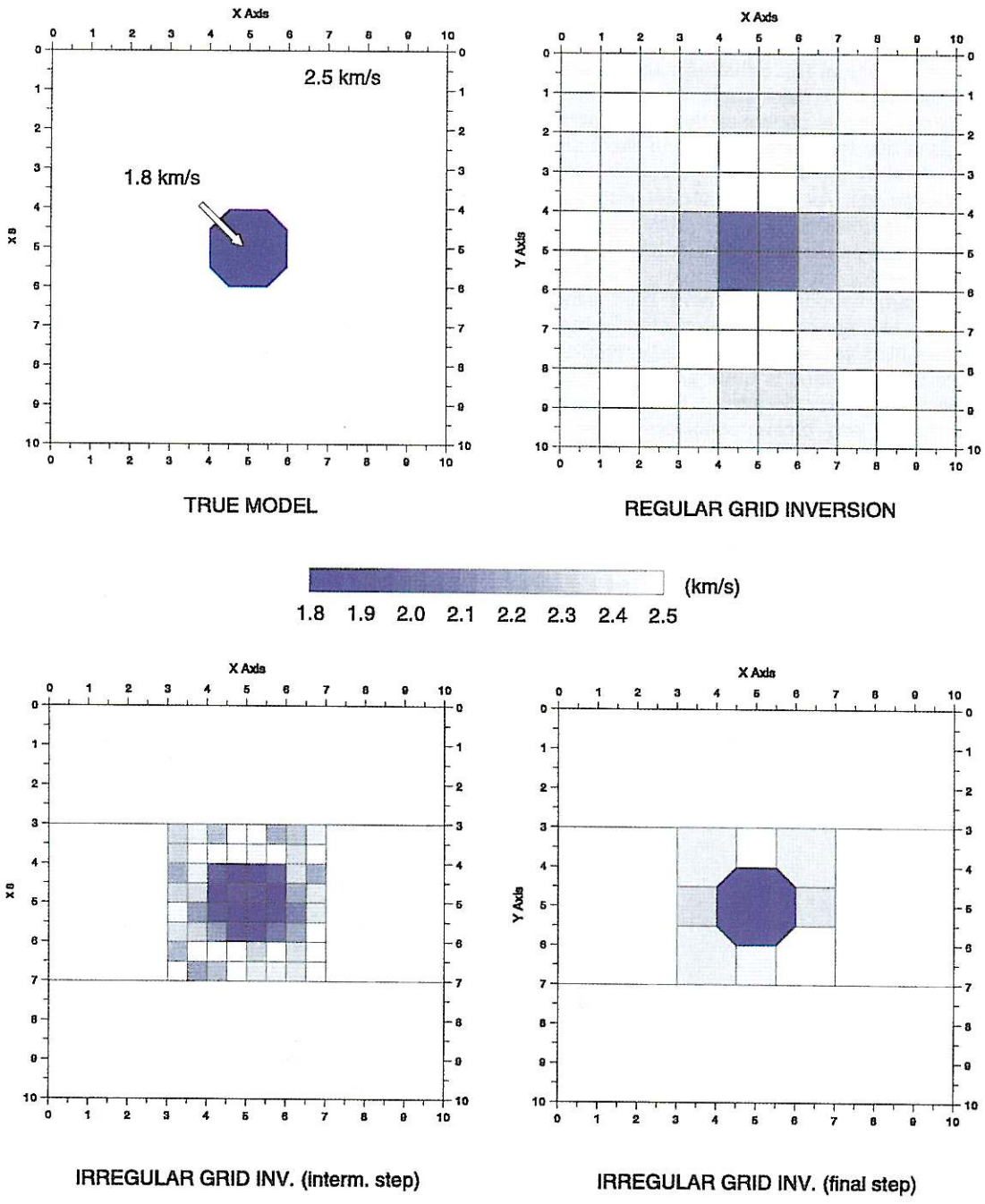

Fig. 9. Horizontal slices at the level of the hydrocarbon trap: true model (top left), tomographic image obtained by a regular grid (top right) and by irregular grids at an intermediate step (bottom left) and the final result (bottom right).

voxels into larger ones, obtains a nearly perfect reconstruction of this 3D object.

Figure 9 allows us to note a basic problem of parametric inversion: the true shape of an irregular anomaly cannot be well approximated by a coarse grid composed by regular rectangles. We obtain a noticeable improvement when the local resolution changes in space, although when rectangles (with a variable size) are used.

Our last result is so good because our model is quite simple and our *a priori* information is correct. As we said before, unfortunately this is not often true. So the following problem arises: how can we adapt our grid to the actual velocity field using only the data, *i.e.* without any *a priori* information?

5. Adaptive regridding

If we do not have any information about the features of the velocity field, a regular grid is an acceptable choice: we distribute the local resolution uniformly, because our ignorance is uniform. But this is not more true after the related tomographic inversion: then we can recover at least some trends of the geological structures. These trends can be exploited to update automatically the initial grid and match better the available rays with the voxel distribution.

Defining a procedure for adaptive regridding, we have to consider different limits. First, the voxel number should be lesser than or equal to that one of the available rays: otherwise the inversion results are affected by the ambiguities due to the null space. Then, we have to increase the local resolution in the zones where the velocity changes; on the other hand, this increase should not introduce a rank-deficiency in the tomographic system (2.1).

Figure 10 is a block diagram of the procedure we propose. Its basic steps are the following:

1) We analyse a preliminary velocity field, obtained for example by a regular grid inversion. (However, any independent geological model or a rough estimate provided by velocity spectra could be used as well). The velocity gradient is computed to reveal possible sharp interfaces, but also the slow spatial changes.

2) We choose some reference points defining the irregular grid, with a density that is higher where the velocity gradient is larger.

3) We check whether these reference points are placed in domains adequately covered by ray paths, and accept only those such that the local reliability in the surrounding domain is high enough.

4) Using the new reference points, we build a new grid and estimate a new velocity field.

5) If the obtained resolution is satisfactory, we stop the procedure, otherwise we go back to step 2 for a further grid refinement.

Given a set of arbitrary reference points, we can define a grid by using two interesting types of voxel shape: the Delauny triangles and the Voronoi polygons. Both may be set up efficiently and are characterised by particular properties. For example, joining the reference point in a Voronoi polygon with those of its

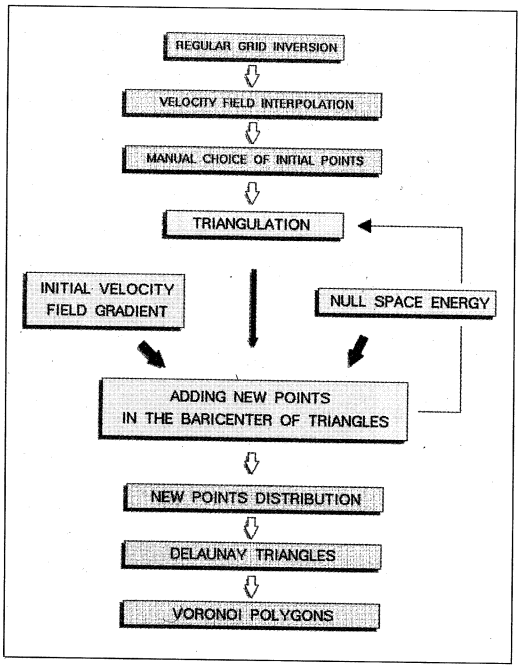

Fig. 10. Block diagram of the procedure for the adaptive regridding.

adjacent polygons, we obtain a (unique) Delauny triangulation. For further details, we refer the reader to Preparata and Shamos (1985).

6. Delauny triangles and Voronoi polygons

We can build a Delauny triangle selecting three points in the set, such that for each of them the two others are the nearest neighbours. An equivalent definition is that the circle passing through the three points does not contain any other point of the whole set. Repeating this operation for all our reference points, we obtain the Delauny triangulation, *i.e.* an irregular grid that can be used for the travel time inversion.

Given a single reference point, the related Voronoi polygon is the domain composed of

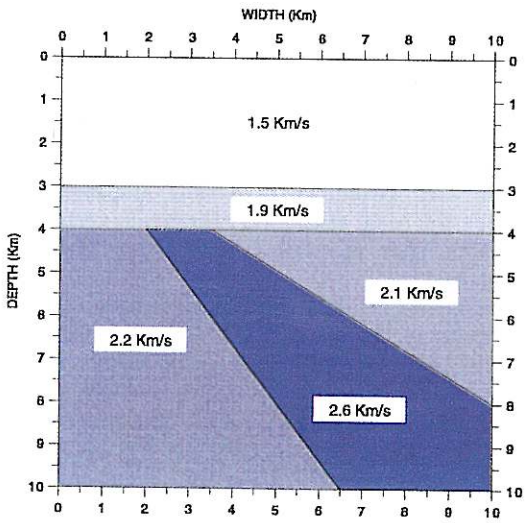

Fig. 11. 2D synthetic model.

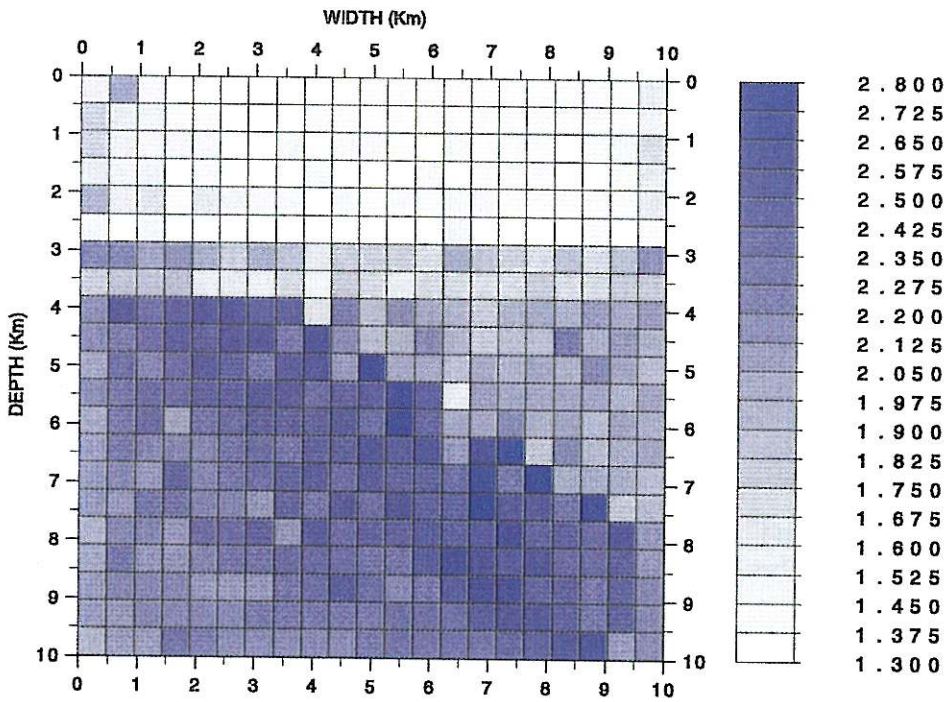

Fig. 12. Tomographic image obtained by a regular grid.

all the points that are closer to it than any other reference point of the set. This polygon is convex, and its boundary can be obtained by a simple procedure. We can take all possible couples composed of our fixed reference point and any other point of the set. They define a line that is equidistant between them, and a half-space that includes the fixed reference point. The intersection of all half-spaces so obtained is its Voronoi polygon.

7. Synthetic example

Figure 11 shows a 2D synthetic model, composed of two horizontal layers overlaying three domains divided by dipping interfaces. We placed 42 source at the left boundary and 42 receivers at the opposite side, all regularly spaced, simulating a cross-well recording of transmitted waves.

A regular grid of dimensions 21 × 21 provides the tomographic image in fig. 12. For the inversion, we adopted a SIRT algorithm without any hard bound, smoothing, or damping factor. Although the major trends are well reconstructed, the interfaces are blurred. For the horizontal ones, this also happens because the voxel limits do not coincide with the interface depth. For the dipping ones, the mismatch between the grid and the actual model cannot be avoided at all.

Figure 13 shows the first part of the procedure for the adaptive regridding. At left we

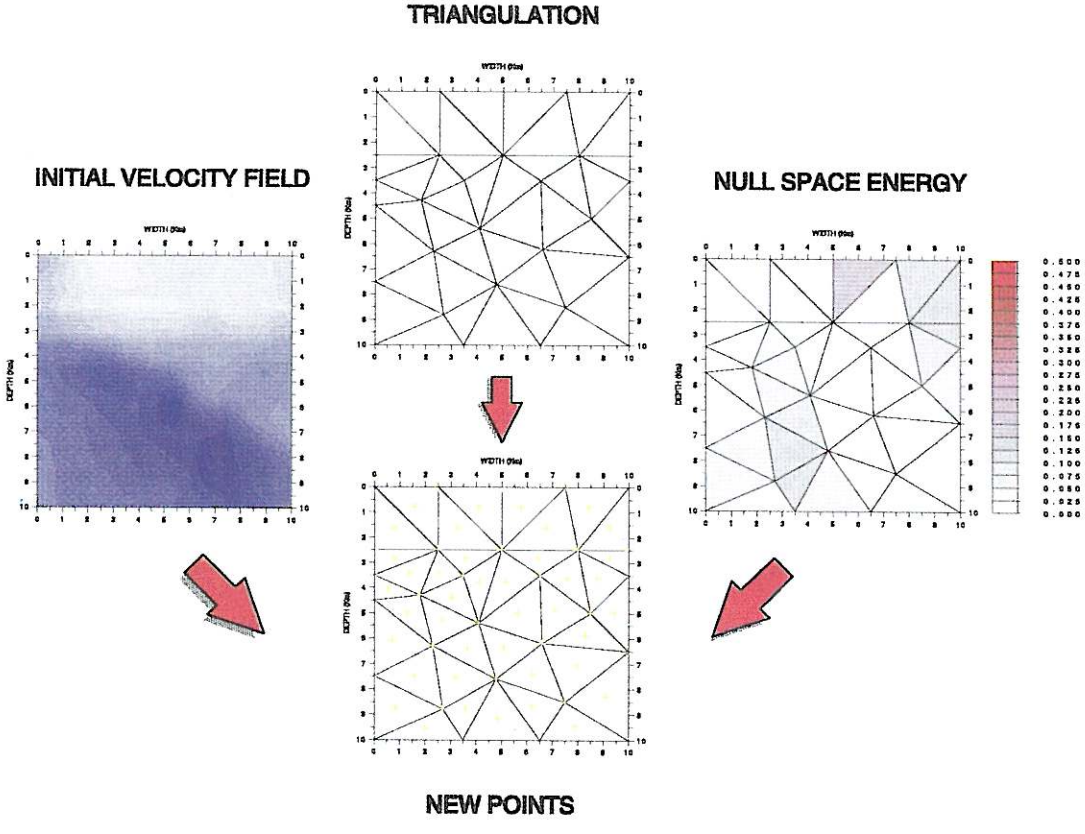

Fig. 13. First iteration for the adaptive regridding.

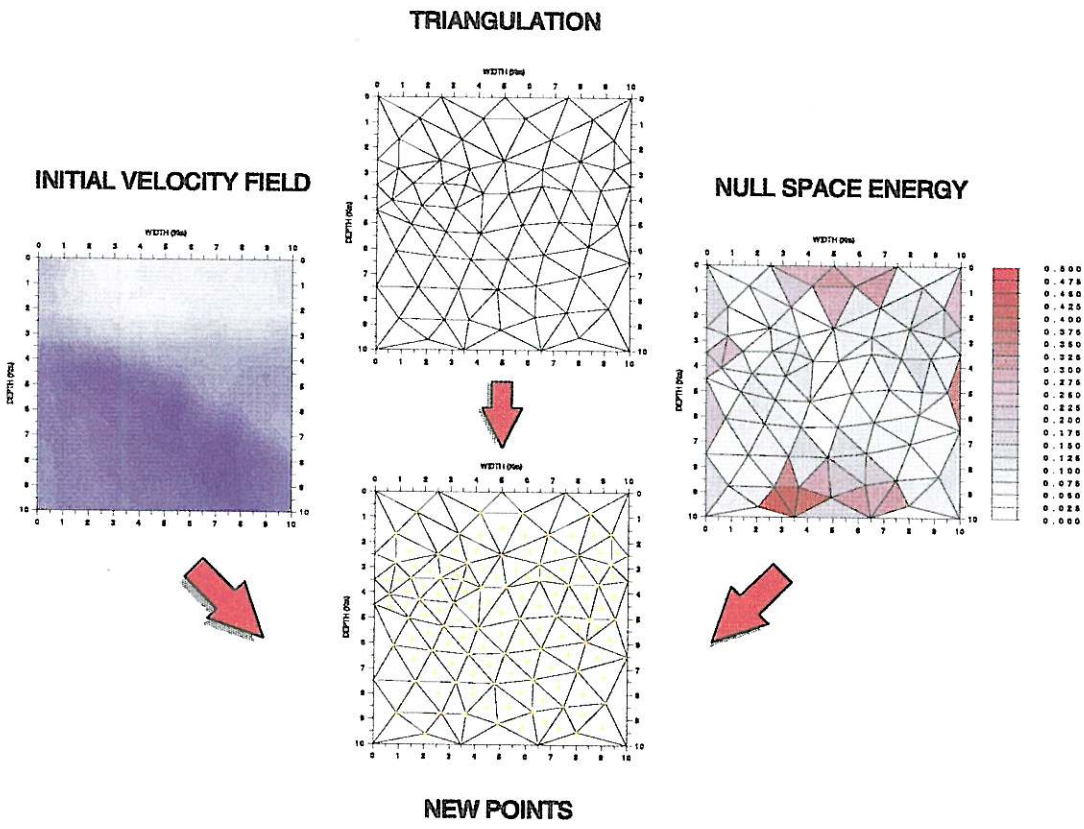

Fig. 14. Second iteration for the adaptive regridding.

see the velocity field obtained by smoothing that one provided by the regular grid. We chose some reference points (top) and, by evaluating the null space energy (right), we add new reference points (bottom), since all present voxels are well constrained by the ray paths.

Repeating the procedure (fig. 14), we notice that some voxels are affected by a too high component of the null space (right), and so we reject the new possible reference points within them. We can go on with the same procedure (fig. 15), increasing the local resolution as far as the null space energy does not exceed a desired threshold.

Figure 16 displays the tomographic image obtained by the Delauny triangles. The two upper horizontal interfaces are well resolved, but the lower dipping interfaces are quite blurred. Much better is the image provided by the Voronoi polygons (fig. 17): all interfaces are clearer and the different domains are much more homogeneous.

We remark that in the last two images the resolution is higher in the central zone, because the ray coverage is better. The voxel number is the same. The regular grid inversion (fig. 12) with a smaller voxel number obtains a much worse image: this happens because the null space is not controlled and the vertical or horizontal voxel sides cannot approximate fairly the dipping interfaces.

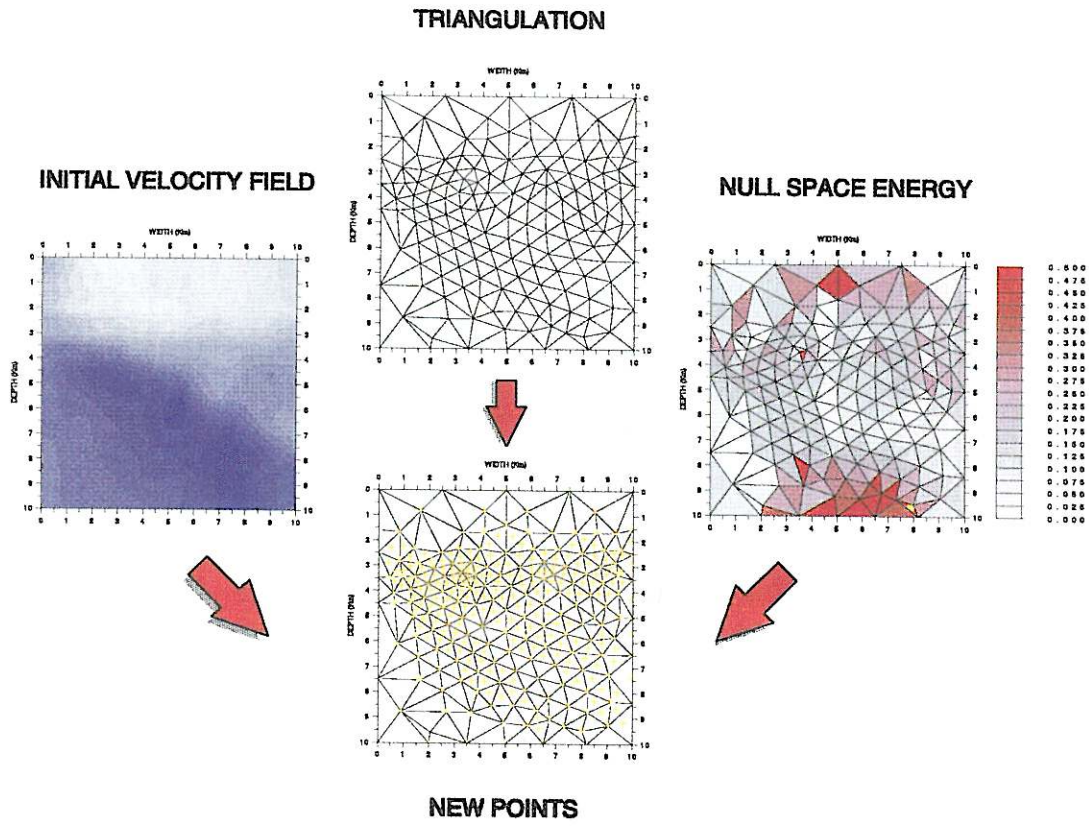

Fig. 15. Third iteration for the adaptive regridding.

8. Conclusions

3D tomographic inversion is a good tool to reconstruct realistic geological structures. Dipping and curved surfaces are usual in structures like synclines and anticlines, direct and reverse faults, salt domes, diapirs and so on. In these cases, the ray path geometries cannot be represented by a 2D model without introducing severe distortions in the travel time estimates, and so in the related tomographic image.

Irregular grids allow the local resolution to be fitted to the available ray paths and to the initially unknown velocity field. These three elements are very closely related: the velocity anomalies bend the rays; the rays crossing the grid provide the tomographic equations; their inversion gives the sought velocity field. This apparently vicious circle can be broken by an iterative procedure. In the standard approach, the ray paths and the velocity anomalies are computed in sequence, leaving the tomographic grid constant and regular. We propose instead to extend this loop by including the adaptive regridding.

Two basic criteria guide our algorithm to search for an optimal grid: first, the null space energy should be minimum; then, we have to reduce the mismatch between the grid shape and the spatial variations of the velocity field. In this way, we defeat the two major causes of blurring, instabilities and ambiguities that are commonly encountered in other approaches.

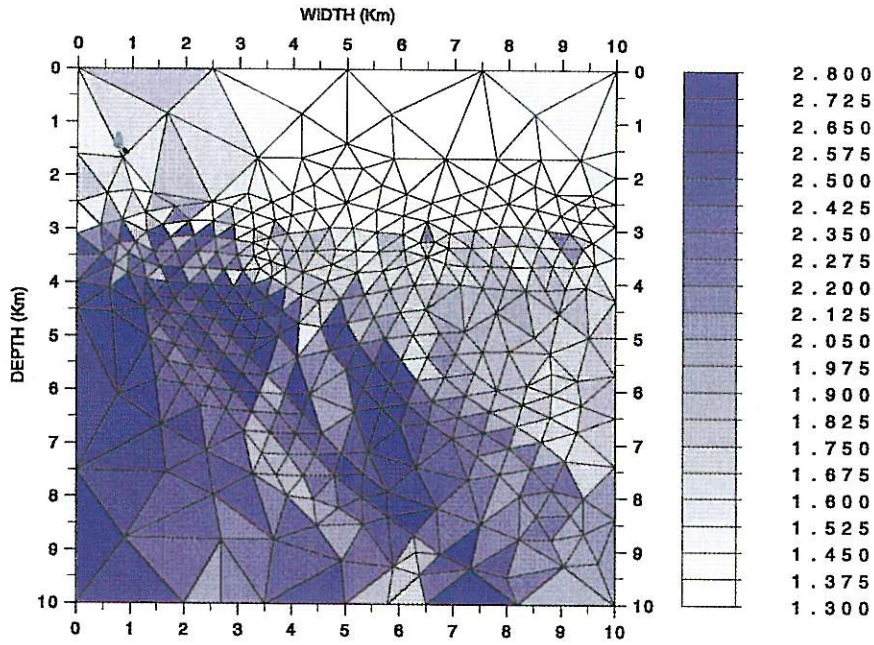

Fig. 16. Tomographic image obtained by the Delauny triangles.

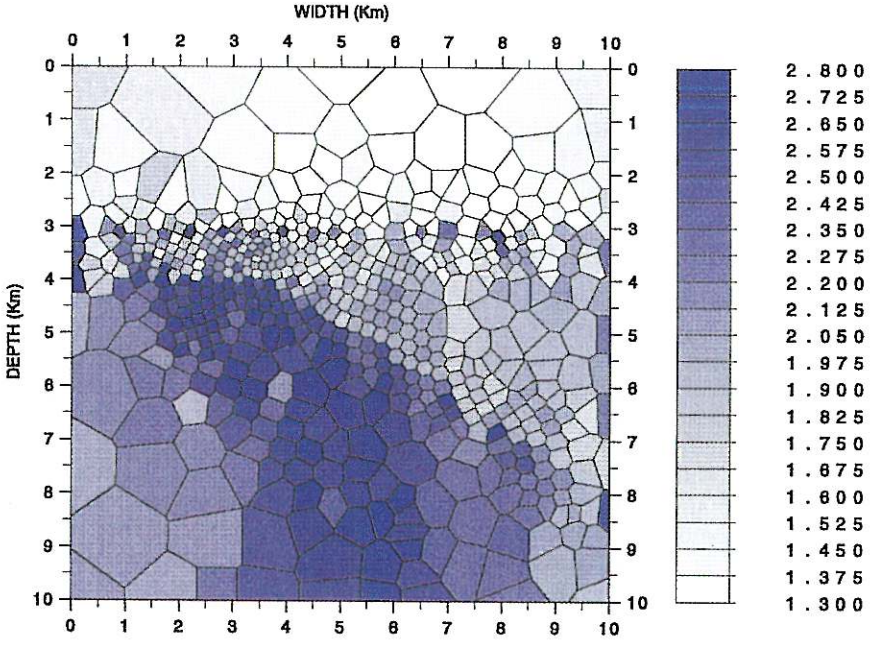

Fig. 17. Tomographic image obtained by the Voronoi polygons.

Acknowledgements

This work was partially supported by the Commission of the European Communities in the Joule 2 Programme (DG XIII, contract No. JOU2-CT93-0321).

REFERENCES

BÖHM, G. and A. VESNAVER (1996): Relying on a grid, *J. Seismic Exploration*, **5**, 169-184.

CARRION, P. (1991): Dual tomography for imaging complex structures, *Geophysics*, **56**, 1395-1376.

CARRION, P., G. BÖHM, A. MARCHETTI, F. PETTENATI and A. VESNAVER (1993a): Reconstruction of lateral gradients from reflection tomography, *J. Seismic Exploration*, **2**, 55-67.

CARRION, P., A. MARCHETTI, G. BÖHM, F. PETTENATI and A. VESNAVER (1993b): Tomographic processing of Antarctica's data, *First Break*, **11**, 295-301.

DOBROKA, M. (1994): Robust optimization methods used in seismic tomography, in *Expanded Abstracts of the 56th EAEG Meeting*, G035.

DOBROKA, M., A. GYULAI, T. ORMOS, J. CSOKAS and L. DRESEN (1991): Joint inversion of seismic and geoelectric data in an underground coal mine, *Geophysical Prospecting*, **39**, 643-665.

HALE, D. (1983): Dip moveout by Fourier transform, *Ph.D. Thesis*, Stanford University.

HUBRAL, P. and T. KREY (1980): Interval velocities from seismic reflection time measurements, SEG, Tulsa.

KACZMARZ, S. (1937): Angenaeherte Aufloesung von Systemen linearer Gleichungen, *Bull. Acad. Polon. Sci. Lett. A.*, **35**, 355-357.

MENKE, W. (1984): *Geophysical Data Analysis: Discrete Inverse Theory* (Academic Press, New York).

PREPARATA, F.P. and M.I. SHAMOS (1985): *Computational Geometry – An Introduction* (Springer Verlag, New York).

ROCCA, F., G. BOLONDI and E. LOINGER (1982): Offset continuation of seismic sections, *Geophys. Prosp.*, **30**, 813-828.

TANER, T. and F. KÖHLER (1969): Velocity spectra – Digital computer derivation and applications of velocity functions, *Geophysics*, **34**, 859-881.

VAN DER SLUIS, A. and H.A. VAN DER VORST (1987): Numerical solution of large, sparse linear algebraic systems arising from tomographic problems, in *Seismic Tomography with Applications in Global Seismology and Exploration Geophysics*, edited by G. NOLET (D. Reidel Publ. Co.).

VESNAVER, A. (1994): Towards the uniqueness of tomographic inversion solutions, *J. Seismic Exploration*, **3**, 323-334.

VESNAVER, A. (1996): The contribution of reflected, refracted and transmitted waves to seismic tomography: a tutorial, *First Break*, **14**, 159-168.

YILMAZ, O. and J.F. CLAERBOUT (1980): Prestack partial migration, *Geophysics*, **45**, 1753-1777.